

Cones-assembled Grating for Long-range Fiber-optic Linear Displacement Sensor

Zeina El Rawashdeh, Philippe Revel, Christine Prella and Frédéric Lamarque

Laboratoire Roberval UMR 7337, Université de Technologie de Compiègne, 60200, Compiègne, France

Keywords: Fiber-optic Sensor, Geometric Modelling, Grating Geometric Design, Diamond Tool Fabrication, Long-range Displacement.

Abstract: This paper presents the initial design of a new fiber-optic displacement sensor; it is used to measure the linear displacement of an actuator performing a helical movement. This sensor consists of a set of assembled cones, which constitute a reflective grating, and two fiber-optic probes. It is characterised by its ability to measure the displacement along a millimetric range, with a high sub-micrometric resolution. In this work, the geometric model of the sensor is presented as well in terms of single probe response in front of a curved reflective surface as in terms of grating shape which authorizes the measurement principle. This grating design makes the displacement measurement possible due to the overlap of the two probes simulated output signals. The single probe measurement in front of a curved reflective surface demonstrates a good agreement with simulation results. A prototype of the cones-assembled grating has been fabricated using a high precision turning machine and a single-crystal diamond tool on an aluminium alloy; the geometric parameters of the fabricated grating were evaluated with the help of a Nanofocus™ µscan optical profilometer. The agreement between the simulated geometric parameters and the real parameters is very good.

1 INTRODUCTION

The need of miniature sensors is becoming essential in modern sciences. Development of micro sensors with high sensitivity, high resolution and high dynamic range dominates the research field for different commercial applications (Mukherjee, 2012). Among the different parameters in numerous applications, is the displacement to be measured with high accuracy, and wide dynamic range.

High resolution and long range contactless displacement sensors are integrated in mechanical systems, where highly precise performances are required. (Fan, 2007) presented the design of a measurement system, consisting of a mini LDGI (linear diffraction grating interferometer) and a focus probe, these two sensors are integrated into the spindle system of a micro/nano-CMM (coordinate measuring machine). The system accuracy is 30 nm for a 10 mm displacement of the spindle.

Fiber-optic technology is chosen for the sensor design because it can achieve contactless measurements within a miniature probe size.

A particular interest in recent studies is to design

miniature fiber-optic displacement sensors with high relative accuracy (nanometric resolution /millimetric range; ratio $\sim 10^{-6}$).

The study developed by (Lee, 2012) presented the design of a fiber-optic displacement sensor with large measurement range; it is composed of a transmissive grating panel, a reflection mirror, and two optical fibers as a transceiver. The measured bidirectional movement demonstrated a peak to peak accuracy of 10.5 μm , high linearity, resolution of 3.1 μm at the full bandwidth, signal-to-noise ratio of 27.7 during a movement of 16004 μm .

To satisfy the requirements of the target application for the sensor, which is the on-line depth measurement for drilled-holes, the surface of the sensor grating must be axis-symmetrical, and consequently the surface has to be curved (convex). (Zhao, 2000) presented a novel fiber-optic sensor for small internal curved surface measurement. The measurement principle is based on beam reflection, and it gives high vertical resolution of 0.1 μm with 8 μm measuring error.

(Patil, 2011) developed a generalised mathematical model able to do the simulation of any

configurations of fiber-optic sensors. It is based on ray tracing approach and different matrix transformations such as translational, reflection or rotational are used. In addition, (Bingshi, 2008) studied the influence of the fiber-optic displacement sensor parameters on its performances, focusing on geometrical parameters such as the numerical aperture, the radius of fiber core, the lateral separation of transmitting and receiving fibers, the angle between the two fibers and the reflector curvature radius. (Utou, 2006) have carried out various experiments in order to verify the effects of various parameters on the accuracy measurement of a fiber-optic displacement sensor, for example: orientation between sensor tip and target surface, i.e. angularity, the effect of varying reflectivity of targets' surfaces, the effect of various transparent material thickness over the target reflective surface and the displacement of a surface in an arc-path away from the stationary tip of a sensor. It was found out that the higher the values of transparent material thickness, the lower the sensitivity values obtained from the fiber-optic sensor probe. The result from the experiment of the angle variation between target and sensor has shown that the sensor sensitivity reduces for angles higher than 20° .

Finally, (Gaikwad, 2012) developed a novel intensity-modulated fiber optic displacement sensor with a convex reflector, in which the sensing structure was described, and the derivations of geometric and Gaussian mathematical models were demonstrated.

This paper introduces first a geometrical model of a convex surface reflector, together with its experimental validation. Then, the modelling of the long-range measurement is done which gives the geometrical parameter of a set of assembled cones which constitute an axi-symmetrical grating. The grating have been fabricated with a high precision turning machine together with a single-crystal diamond tool, in order to obtain high geometric precisions and a good surface quality ($R > 95\%$, polished-mirror surface).

These fabricated cones have been geometrically characterised for future use of the sensor, where high performances regarding its sensitivity, measurement range and resolution are required for online depth measurement while machining.

2 SENSOR PRINCIPLE

The sensor consists of two fiber-optic probes

associated to a high reflective surface. Each probe has one emission fiber and four reception fibers. The sensor performances when it is associated to a planar surface have been already analysed (Alayli, 1998, Girão 2001). When translating the flat mirror perpendicularly to the probe axis, the sensor response curve is obtained (Figure 1).

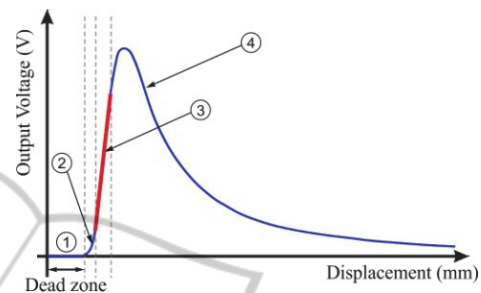


Figure 1: Response curve of the fiber-optic displacement sensor.

The preferred working zone of the sensor is zone (3) because of its linearity and high sensitivity. However, the measurement range of this zone is too small ($< 200 \mu\text{m}$). So, in order to increase the linear zone, the displacement direction of the flat mirror is different from the normal vector orientation of its surface resulting in the multiplication of the nominal range value by $(\sin \epsilon)^{-1}$ factor where ϵ is the inclination angle related to the grating axis. By repeating the tilting mirror configuration, a grating is obtained. For an inclination angle ϵ of several degrees, the sensor resolution can be reached to 15 nm and the measurement range can be increased to several millimeters as a function of the grating steps number. It is possible to do long-range measurements if the non-linear signal during the transition between two consecutive steps is avoided. To do so, two probes are used, to ensure a continuous displacement measurement over the long-range by alternately switching between the probes in order to avoid strong non-linearity due to the illumination of two grating steps at the same time. A sensor prototype was successfully modelled, designed and tested (Prelle, 2006).

The objective of the current work is to develop a sensor able to measure precisely the linear displacement of an actuator performing a helical movement. For this new application, the sensor

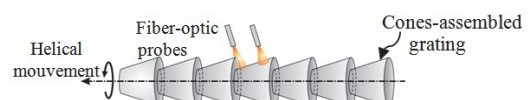


Figure 2: Measurement principle with a 3D grating.

reflective grating has to have a 3D shape in order to provide a valid measurement even if the sensor rotates along its axis of symmetry, as shown in the figure 2.

3 GEOMETRIC MODEL OF THE REFLECTIVE SURFACE

3.1 Convex Surface Modelling

The influence of the curved reflector on the sensor performances was modelled. The reflective grating of the sensor is a set of assembled cones, which implies that the sensor reflector surface is convex. This property will modify the sensor performances as compared to the previous existing sensor with grating composed of an assembly of flat mirrors (Prelle, 2006, Khat 2010). In order to observe the influence of the convex surface on the sensor performances, different geometric parameters were considered. These parameters are shown in Table 1 and figure 3.

Table1: Geometric model parameters.

Symbol	Definition
\emptyset	The probe diameter (mm)
R_c	Radius of curvature (mm)
M	Tangential point
\vec{n}_M	Normal vector to tangent
d_0	Initial distance between the reflector and the probe (mm)
α	The incidence angle
δ	The angle between \vec{n}_M and the symmetrical axis of the probe
e	The spacing between the emission fiber and the reception fiber
Δ	The spacing between the normal vector of the flat surface and the reflected beam from the curved surface intercepted by the sensor

The aim of this theoretical model is to analyse the sensor performances when it is associated to a convex reflector, and compare these performances to a planar reflector. For that, the response curve of the sensor was generated in the two cases (Flat surface and convex surface), by detecting the light intensity of the sensor as a function of the displacement (d_0) and the radius of curvature (R_c).

In the model two conditions were taken into account to ensure that the light is detected by the sensor.

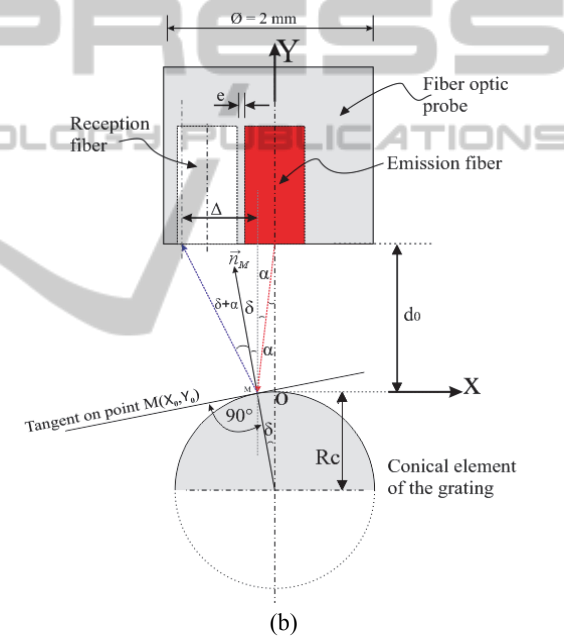
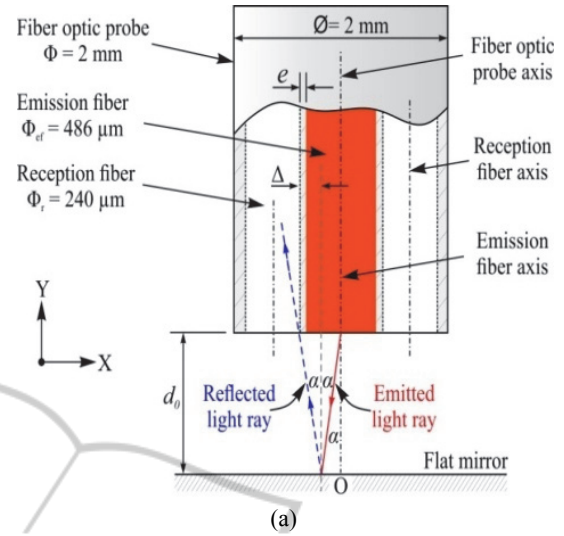


Figure 3: Schematic diagram of the reflected light model: (a) Flat mirror, (b) convex mirror.

These conditions are illustrated in the following equations:

$$\alpha < \beta - 2 \times \delta \quad (1)$$

$$R_{\text{emission}} + e < X_0 + \Delta < R_{\text{emission}} + e + D_{\text{reception}} \quad (2)$$

Where $\beta = \arcsin(0.46)$, α and δ are defined in Table 1, R_{emission} is the radius of the emission fiber, and $D_{\text{reception}}$ is the diameter of the reception fiber. The variables δ and Δ are calculated geometrically for each point (X_0, Y_0) .

Figure 4 represents the results of several radii of curvature (R_c) as a function of the displacement (d_0).

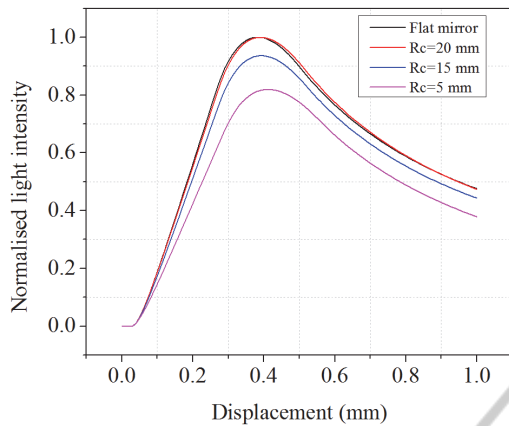


Figure 4: Response curves for several radii of curvature.

The flat mirror configuration is used as the reference. It is clear that the higher the radius of curvature is, better will be the normalised light intensity detected in the linear part of the curve, in consequence, better will be the sensor performance. For $R_c = 15$ mm, the signal light intensity reduces sharply.

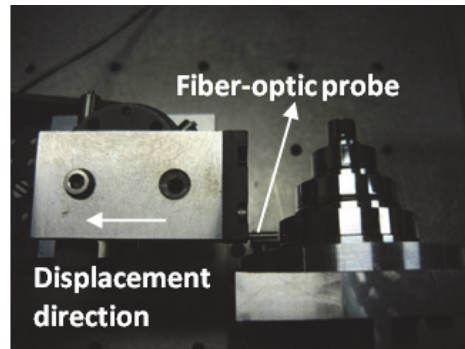
Table 2 represents the loss in sensitivity ratio (Att) due to the convex form of the reflector, as a function of different radii of curvature, where:

- Att : The loss in sensitivity ratio
- S_{RC} : The linear sensitivity of a curved reflector (mm^{-1})
- S_{∞} : The linear sensitivity of a planar reflector

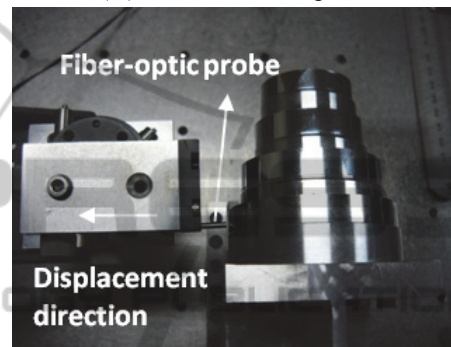
3.2 Experimental Validation of the Convex Surface Modelling

The geometric model previously described has been validated experimentally by fabricating two pieces of cylinders with different diameters: Piece (A) with small diameters (40, 30, 20, 10 mm) and piece (B) with large diameters (55, 50, 40, 35 mm). These two pieces have been fabricated with a single crystal diamond tool on a high precision turning machine whose characteristics and performances are described in section 5.

For each cylinder in the two pieces, the calibration curve of the sensor has been obtained by moving the sensor away from the cylinder reflecting surface. The linear sensitivity has been calculated for each curve, with a linearity criterion of 1 %. Figure 5 illustrates the experimental set-up used; it consists of the two reflecting pieces together with a fiber – optic probe.



(A): small diameter piece



(B): large diameter piece

Figure 5: Experimental set-up.

Table 2: Loss in sensitivity

R_c (mm)	1	5	10	15	20	∞
$\frac{Att}{S_{RC}} = \frac{S_{RC}}{S_{\infty}}$	0.7	0.74	0.8	0.91	0.98	1

The experimental sensitivities (zone 3 of figure 1) have been compared to the theoretical sensitivities in

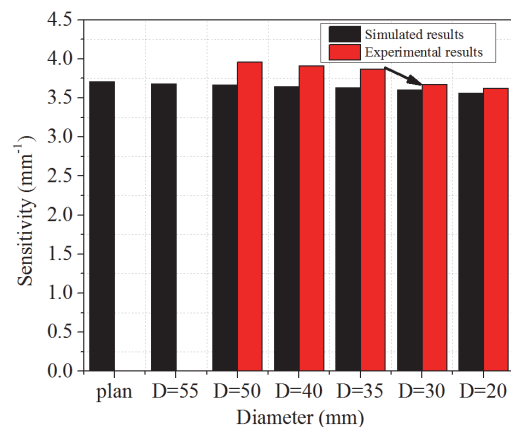


Figure 6: Influence of the diameter of the reflective convex surface on the sensor sensitivity.

order to test the precision of the geometric model (Figure 6).

The previous figure illustrates the influence of the cylinder diameter on the linear sensitivity of the sensor (simulated and experimental). It reduces as the cylinder diameter decreases.

This experiment validates the geometric model and shows that it is preferred to have a diameter higher than 35 mm for applications requiring high sensitivity.

For the mentioned reasons, and to guarantee a good performance of the sensor, the cones-assembled grating has been fabricated from a 50 mm diameter cylinder.

4 GRATING GEOMETRICAL DESIGN

A geometrical model was developed to simulate the functioning of the long-range displacement sensor. As a result, the optimal dimensions for each step of the grating are provided. These dimensions ensure the measurement continuity over a millimetric range with a sub-micrometric resolution. This geometrical model takes into account the following two conditions:

1. The distance between the probe and the grating step has to be in the linear zone (zone 3 of figure 1).
2. The overlap between two successive signals is fixed at $30 \mu\text{m}$ to avoid the linear measurement discontinuity during the steps transition.

The grating geometrical model is based on the algorithm shown in figure 7.

Figure 8 shows the geometric parameters considered for a step in the cones-assembled grating, where:

- l : The step length (μm)
- h_p : The step height (μm)
- ε : The step angle ($^\circ$)
- γ : the angle at the bottom of the step ($^\circ$)

The model optimizes the dimensions to get the best limit of resolution which depends on the value of ε . The more ε is, the smallest will be the limit of resolution. Figure 8 shows the successive algorithm sequences used to simulate the functioning of the measurement principle. The geometric model of the convex surface explained above leads to the best limit of resolution of a single fiber-optic probe used as a simple displacement sensor.

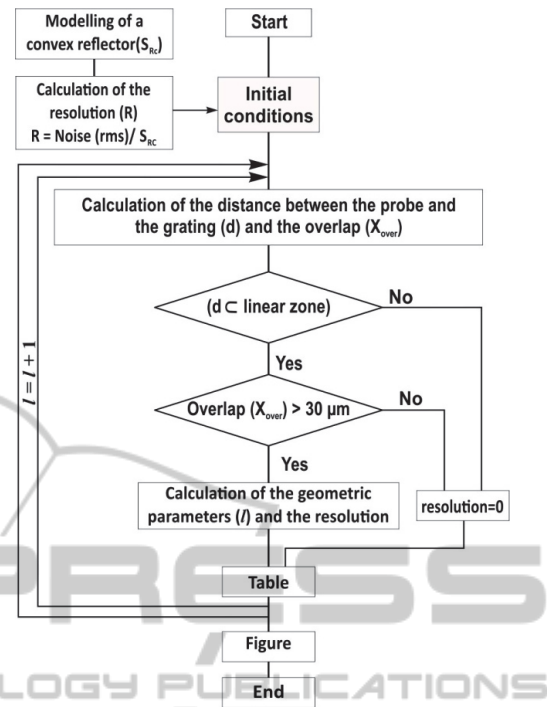


Figure 7: Algorithm of the geometrical model.

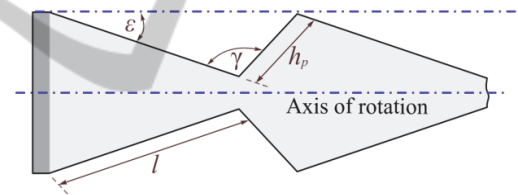


Figure 8: Geometrical parameters of the cones-assembled grating.

The algorithm figured out the values of each geometric parameter:

- The step length (l) is $1541 \mu\text{m}$
- The segment (h_p) is $253 \mu\text{m}$
- The angle (γ) is 130°
- The step angle ε is 7.17°

The theoretical limit of resolution is 24 nm with an overlap between the two signals of $30 \mu\text{m}$.

Figure 9 shows the theoretical displacements calculated with Matlab software, where:

- Theoretical axial position (μm): The position of the sensor in the classical case (without inclination)
- Theoretical lateral position (μm): The position of the sensor in the lateral case (with inclination)

It is clear that the lateral displacement range

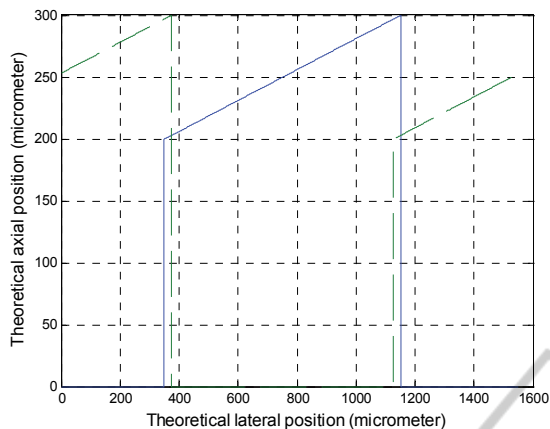


Figure 9: Theoretical axial position (μm) vs. theoretical lateral position (μm).

(801.0 μm) is higher than the axial one (100.1 μm), by a factor of $\sin 7.17^\circ$.

5 CONICAL GRATING FABRICATION

After the geometrical model phase, the fabrication technique has to be taken into account, and that includes the performances of the turning machine, as well as the fabricating tool whose geometrical design, particularly, its radius of curvature influences the fabrication procedure and its final product.

A machining program has been used, in which all these constraints have been taken into consideration.

5.1 Fabricating Elements Characteristics

In the case of 3D axis – symmetrical pieces, the high precision rotating spindle coupled with single crystal diamond tool provide high geometrical precisions as well as good surface qualities. That is important for the sensor based on cones-assembled grating, where the light reflection influences the sensor sensitivity and range.

The machine used for the fabrication technique is a high precision turning machine (Figure 10).

The machine is a prototype lathe with T slide architecture. On the Z-axis a magnetic bearing spindle is fixed, and on the X-axis is fixed the tool holder. The two hydrostatic slides (X and Z) are fixed on a 1.5 ton granite block; this block is

supported by a high frequency vibration-filtration system.

The hydrostatic bearings minimise the friction forces to ensure a high rigidity as well as a straight tool trajectory. For each axis, the straightness error is 0.3 μm for a total displacement of 100 mm.

The two slides are actuated with the help of two linear motors; the displacement is measured by an optical encoder with a 4 nm limit of resolution.

The two motors are controlled numerically with the help of PMAC card.

On the Z-axis, a high precision rotating spindle is fixed together with magnetic bearings in order to avoid friction loss and to ensure the right trajectory during rotation.

This machine proved highly geometrical precisions regarding the dimensions of the fabricated pieces as well as high surface qualities (Gautier, 2008).

In order to obtain high surface roughness less than 15 nm, it is preferred to use a single – crystal diamond tool, thanks to its good qualities, such as: hardness, good thermal conductivity and the low waviness of the cutting edge (Yuan, 1996).

An aluminium alloy 2017 has been used to fabricate the grating.

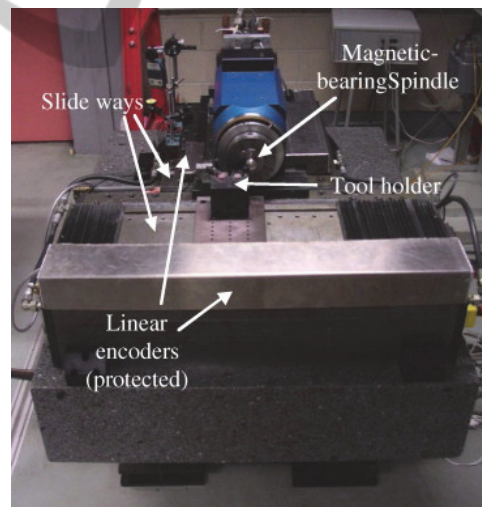


Figure 10: High precision turning machine.

5.2 Influence of the Tool Radius of Curvature on the Geometry

The radius of curvature of the fabricating tool has not been considered in previous studies. The more it is sharp; the better will be the step profile at the bottom of the steps (Figure 11). In the actual prototype, this angle (γ) was fixed at 130° . However, when the value of the angle γ is too high, the non-

useful zone of the grating at the bottom of the steps will increase. As a consequence, in future works, the value of γ has to be optimised between 90° and 130° which will enhance the sensor performance.

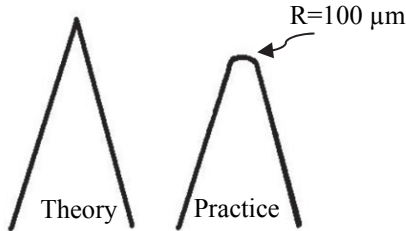


Figure 11: The tool radius of curvature.

5.3 Description of the Machining Program

In order to have a good surface roughness for the sensor grating, the depth cut has to be between 5 and 10 μm (Gautier, 2008).

The machining program is divided into two main parts: In the first part, every step is machined by achieving seven successive cuts (Figure 12). The second part is the last finishing cut which allows getting the final form of the overall grating.

In this prototype, ten steps were machined to generate the sensor reflector grating.

For every step, two successive trajectories were programmed: Firstly, from point A to point B as shown in the figure 12 in order to get into the material and to generate a slope respecting the value of the angle ϵ . The second trajectory is from point B to point C (Figure 12) to get out from the material following the angle γ . Afterwards, the tool turns back to its initial position A to re-do another cut.

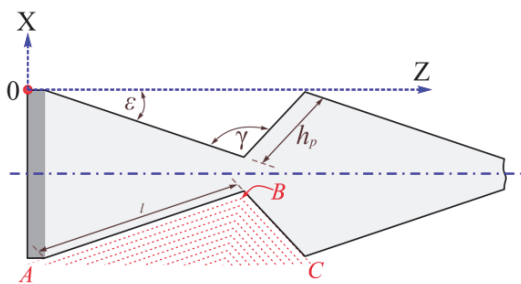


Figure 12: Machining technique.

However, the contact point between the tool cutting edge and the material as well as the tool radius of curvature, both are not the same in the two successive trajectories (Figure 13).

In the first six cuts, the depth was fixed to 20 μm . The seventh cut was done at 10 μm .

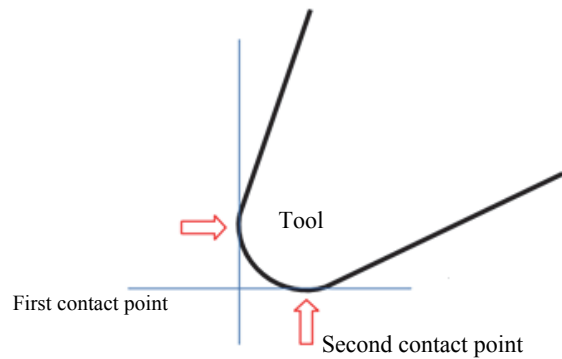


Figure 13: Machining contact points.

The length of the first trajectory has been reduced by 5 μm so that during the last finishing cut (the 8th), the depth of the machined material is at 5 μm of precision which ensures optimal cutting conditions.

At the last finishing cut, the depth in the first trajectory has been fixed at 5 μm .

The lubrication flow has been increased and finally the feedrate speed was decreased to 50 $\mu\text{m/s}$, in order to obtain a high surface quality (polished-mirror).

6 GEOMETRICAL CHARACTERISATION OF THE FABRICATED CONES

A grating prototype has been fabricated using the single-crystal diamond tool, following the described program in order to reach the theoretical dimensions identified in the geometric model (Figure 14).

This fabricated grating have been characterised geometrically using the NanofocusTM μscan optical profilometer to measure the steps profiles and compare them to the theoretical dimensions (Figure 14).

Figure 15 shows the profile of the measured grating. The average value of the angle ϵ on the ten

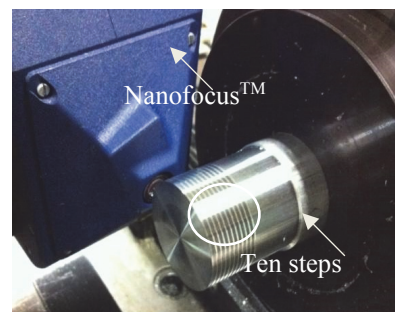


Figure 14: Geometrical characterisation of the grating using the Autofocus sensor.

steps is 7.25° .

The average of the measured height is ($196.2 \pm 2.1 \mu\text{m}$) for a theoretical height of $194 \mu\text{m}$, the average of the measured length is ($1539.6 \pm 4.1 \mu\text{m}$) for a theoretical one of $1541.8 \mu\text{m}$.

These results are very good for an initial prototype.

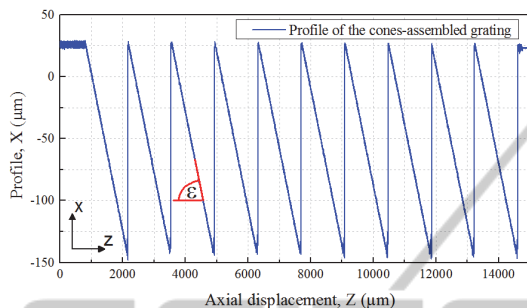


Figure 15: Profile of the measured steps after fabrication.

7 CONCLUSIONS

This paper presents the design of an original fiber-optic displacement sensor, which will be used to measure the linear displacement of an axis performing a helical movement.

First, the geometric model of the sensor principle was presented in order to obtain the theoretical geometric parameters. These parameters lead to the optimal cones-assembled grating, masterpiece of the long-range displacement measurement principle.

Then, a 10 steps grating prototype of the sensor was fabricated using a high precision turning machine with the help of a single crystal-diamond tool on an aluminium alloy in order to obtain high precision in the fabricated dimensions, as well as high reflectivity which ensures good sensor sensitivity and linearity.

The conical grating prototype was characterised using Nanofocus™ µscan optical profilometer and the measured parameters are close to the theoretical ones.

In a near future, this grating will be used together with two fiber-optic probes to measure on-line the translation of an axis along several millimeters when the measuring head of the spindle rotates at 360° during the translation.

ACKNOWLEDGEMENTS

The Authors would like to thank Cetim (Centre

Technique des Industries Mécaniques) for the support of this work.

The authors would like to thank B. Bosschaert, N. Delias and P. E. Karcher, students in University of technology of Compiègne, for their help in the fabrication of the conical grating.

REFERENCES

- T. Mukherjee, T.K. Bhattacharyya, 2012. A Miniature, High Sensitivity, Surface Micro-machined Displacement Sensor with High Resolution. *The 2012 IEEE/ASME International Conference on Advanced Intelligent Mechatronics, Kaohsiung, Taiwan*.
- K.C. Fan, Z. F. Lai, P. Wu, Y. C. Chen, Y. Chen, G. Jager, 2007. A displacement spindle in a micro/nano level, *Measurement Science and Technology* doi :10.1088/0957-0233/18/6/S07.
- A. D. Gaikwad, J. P. Gawande, A. K. Joshi, R. H. Chile, 2012. An Intensity-modulated optical fibre displacement sensor with convex reflector, *International journal of advanced research in electrical, electronics, and instrumentation engineering, vol. 1, Issue 1*.
- Y.G. Lee, Y.Y. Kim, C.G. Kim, 2012. Fiber optic displacement sensor with a large extendable measurement range while maintaining equally high sensitivity, linearity, and accuracy. *Review of Scientific Instruments* 83, 045002(2012); doi: 10.1063/1.3698586.
- Y. Zhao, P. Li, C. Wang, Z. Pu, 2000. A novel fiber-optic sensor for small internal curved surface measurement. *Sensors and Actuators A, vol. 86, pp. 211-215*.
- S.S. Patil, A.D. Shaligram, 2011. Modeling and experimental studies on retro-reflective fiber optic micro-displacement sensor with variable geometrical properties. *Sensors and Actuators A, Vol. 172, pp. 428-433*.
- X. Bingshi, X. Wen, Y. Dong, 2008. A theoretical analysis on parameters of fiber optic displacement sensor. *Proc. of SPIE, Vol. 7129, pp. 1-6*.
- F. E. Utou, J. Gryzagoridis, B. Sun, 2006. Parameters affecting the performance of fiber optic displacement sensors. *Smart Mater. Struct.* 15 (2006) S154-S157, doi: 10.1088/0964-1726/15/1/025.
- Y. Alayli, D. Wang, M. Bonis, 1998. Optical fiber profilometer with submicronic accuracy. *Proc. SPIE, 3509*.
- P.M.B.S. Girão, O.A. Postolache, J.A.B. Faria, J.M.C.D. Pereira, 2001. An overview and a contribution to the optical measurement of linear displacement, *IEEE Sens. J. pp. 322-331*.
- C. Prella, F. Lamarque, P. Revel, 2006. Reflective optical sensor for long-range and high-resolution displacements. *Sensors and Actuators A, vol. 127*.
- A. Khiat, F. Lamarque, C. Prella, Ph. Pouille, M. Leester-Schadel and S. Büttgenbach, 2010. Two-dimension fiber optic sensor for high-resolution and long

range linear measurements. *Sensors and Actuators A*, vol. 158, Issue 1.

A. Gautier, H. Khanfir, P. Revel, R.Y. Fillit, 2008. Polish-mirror finish surfaces obtained by high precision turning, *Int. J. Machining and Machinability of Materials*, Vol. 4, Nos. 2/3.

Z.J. Yuan, M. Zhou, S. Dong, 1996. Effect of diamond tool sharpness on minimum cutting thickness in ultraprecision machining, *J. Mater. Proc. Tech.* 62 (4), pp. 327–330.

